

# Exciton Dissociation Dynamics in Model Donor-Acceptor Polymer Heterojunctions: I. Energetics and Spectra

Eric R. Bittner,\* John Glenn Santos Ramon, and Stoyan Karabunarliev  
*Department of Chemistry and Center for Materials Chemistry,*  
*University of Houston*  
*Houston, TX 77204*  
 (Dated: June 8, 2018)

In this paper we consider the essential electronic excited states in parallel chains of semiconducting polymers that are currently being explored for photovoltaic and light-emitting diode applications. In particular, we focus upon various type II donor-acceptor heterojunctions and explore the relation between the exciton binding energy to the band off-set in determining the device characteristic of a particular type II heterojunction material. As a general rule, when the exciton binding energy is greater than the band off-set at the heterojunction, the exciton will remain the lowest energy excited state and the junction will make an efficient light-emitting diode. On the other hand, if the off-set is greater than the exciton binding energy, either the electron or hole can be transferred from one chain to the other. Here we use a two-band exciton to predict the vibronic absorption and emission spectra of model polymer heterojunctions. Our results underscore the role of vibrational relaxation and suggest that intersystem crossings may play some part in the formation of charge-transfer states following photoexcitation in certain cases.

## I. INTRODUCTION

Organic semiconducting polymers are currently of broad interest as potential low-cost materials for photovoltaic and light-emitting display applications. While research into the fabrication, chemistry, and fundamental physics of these materials continues to advance, devices based upon organic semiconductors have begun to appear in the market place. Composite materials fabricated by mixing semiconducting polymers with different electron and hole accepting properties have been used to make highly efficient solar cells and photovoltaic cells.[1, 2, 3] The advantage gained by mixing materials is that when a conjugated polymer material absorbs light, the primary species produced is an exciton, i.e. an electron/hole pair bound by Coulombic attraction, rather than free charge carriers. As a result, a single layer conventional Schottky-barrier cell of a molecular semiconductor sandwiched between two metal electrodes has poor power conversion and charge collection efficiencies. In composite materials, the driving force for charge separation is due to the mismatch between the HOMO and LUMO levels of the blended materials. This creates a band off-set at the interface between the two materials. A type I heterojunction is when the HOMO and LUMO levels of one of the materials both lie within the HOMO-LUMO gap of the other. A type II heterojunction occurs when both the HOMO and LUMO of one material are simultaneously shifted up or down relative to the HOMO and LUMO levels of the other material. By and large, organic semiconductor heterojunctions fall into the type II category.[4] The chemical structure of some of the more important materials for device applications are shown in Fig. 1.

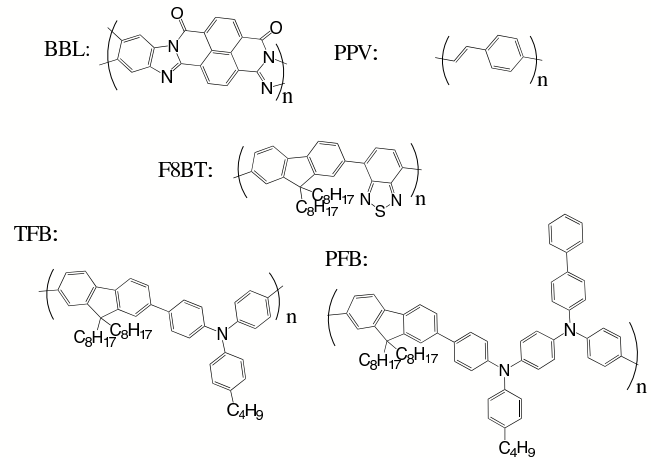


FIG. 1: Chemical structure of the various conjugated polymers considered in this paper.

Photocurrent production within a type II material hinges upon its ability to dissociate the bound electron/hole pairs produced by photoexcitation. To a first approximation, the dissociation threshold is determined by the ratio of the exciton binding energy,  $\varepsilon_B$ , to the band off-set at the heterojunction,  $\Delta E$ . If  $\Delta E > \varepsilon_B$ , the exciton will be energetically unstable and can undergo fission to form charge-separated states and eventually free charge carriers. On the other hand, when  $\Delta E < \varepsilon_B$ , the exciton remains the favorable species. For typical organic semiconductors,  $\varepsilon_B \approx 0.5 - 0.6$  eV. In heterojunctions composed of poly(benzimidazobenzophenanthroline ladder) (BBL) and poly(1,4-phenylenevinylene) (PPV),  $\Delta E$  is considerably greater than  $\varepsilon_B$ [5]. As a result, recent reports of devices fabricated from nanoscale layers of BBL and PPV or its derivative poly(2-methoxy-5(2"-ethylhexyloxy)-1,4-phenylenevinylene) (MEH-PPV) indicate

\*email:bittner@uh.edu

very efficient photoinduced charge transfer and large photovoltaic power conversion efficiencies under white light illumination.[6, 7, 8]

Surprisingly, type II materials can also be used to produce highly efficient light-emitting diodes (LEDs). In demixed blends of poly(9,9-dioctylfluorene-co-benzothiadiazole) (F8BT) and poly(9,9-dioctylfluorene-co-N-(4-butylphenyl) diphenylamine) (TFB), the exciton is the stable species and fabricated devices show excellent LED performance[9]. While chemically similar to TFB, blends of F8BT with poly(9,9-dioctylfluorene-co-bis-N,N-(4-butylphenyl)-bis-N,N-phenyl-1,4-phenylenediamine) (PFB) exhibit very poor LED performance. Changing the diphenylamine to a phenylenediamine within the co-polymer shifts the position of the HOMO energy level by +0.79 eV relative to the HOMO level of TFB. (Table I) and destabilizes the exciton.

In this paper we investigate the role of interchain coupling and lattice reorganization in determining the essential states model polymer semiconductor systems consisting of parallel chains of PPV:BBL, TFB:F8BT, and PFB:F8BT. In the case of the PPV:BBL heterojunction, the exciton binding energy is smaller than the band offset leading to electron transfer from the photoexcited PPV to the BBL chain. In the case of TFB:F8BT and PFB:F8BT junctions, the band off-sets are close to the exciton binding energy and we see considerable mixing between intramolecular excitonic states with intermolecular charge-transfer or exciplex states. Moreover, in TFB:F8BT, avoided crossing between Born Oppenheimer potential energy surfaces may open channels for exciton regeneration that are thermally accessible from the exciplex states as recently reported by Morteani *et al.*[10]. In a subsequent paper we will report upon our simulations of the charge-injection and photoexcitation dynamics within these systems. [11]

TABLE I: Band centers and reported HOMO and LUMO levels for various polymer species. Parenthesis indicate the modulation of the intramolecular valence and conduction band site energies.

Molecule	$\varepsilon_e$	$\varepsilon_h$	HOMO	LUMO
PPV	2.75 eV	-2.75 eV	-5.1 eV <sup>1</sup>	-2.7 eV <sup>1</sup>
BBL	1.45	-3.55	-5.9 <sup>1</sup>	-4.0 <sup>1</sup>
F8BT	1.92 (2.42,1.42)	-3.54 (-3.04,-4.04)	-5.33 <sup>2</sup>	-3.53 <sup>2</sup>
PFB	3.16 (3.36,2.96)	-2.75 (-2.55,-2.95))	-5.1 <sup>2</sup>	-2.29 <sup>2</sup>
TFB	3.15 (3.35,2.95)	-2.98 (-2.78,-3.18)	-5.89 <sup>2</sup>	-2.30 <sup>2</sup>

1.) M. M. Alam and S. A. Jenekhe, Chem. Mater. **16**, 4647 (2004). 2.) A. C. Morteani, P. Sreearunothai, L. M. Herz, R. H. Friend, and C. Silva, Phys. Rev. Lett. **92**, 247402 (2004).

## II. THEORETICAL APPROACH

Our basic description is derived starting from a model for the on-chain electronic excitations of a single conjugated polymer chain.[12, 13, 14] This model accounts for the coupling of excitations within the  $\pi$ -orbitals of a conjugated polymer to the lattice phonons using localized valence and conduction band Wannier functions ( $|\bar{h}\rangle$  and  $|p\rangle$ ) to describe the  $\pi$  orbitals and two optical phonon branches to describe the bond stretches and torsions of the the polymer skeleton.

$$\begin{aligned}
 H = & \sum_{\mathbf{mn}} (F_{\mathbf{mn}}^\circ + V_{\mathbf{mn}}) A_{\mathbf{m}}^\dagger A_{\mathbf{n}} \\
 & + \sum_{\mathbf{nm}i\mu} \left( \frac{\partial F_{\mathbf{nm}}^\circ}{\partial q_{i\mu}} \right) A_{\mathbf{n}}^\dagger A_{\mathbf{m}} q_{i\mu} \\
 & + \sum_{i\mu} \omega_\mu^2 (q_{i\mu}^2 + \lambda_\mu q_{i\mu} q_{i+1,\mu}) + p_{i\mu}^2 \quad (1)
 \end{aligned}$$

where  $A_{\mathbf{n}}^\dagger$  and  $A_{\mathbf{n}}$  are Fermion operators that act upon the ground electronic state  $|0\rangle$  to create and destroy electron/hole configurations  $|n\rangle = |\bar{h}p\rangle$  with positive hole in the valence band Wannier function localized at  $h$  and an electron in the conduction band Wannier function  $p$ . Finally,  $q_{i\mu}$  and  $p_{i\mu}$  correspond to lattice distortions and momentum components in the  $i$ -th site and  $\mu$ -th optical phonon branch. Except as noted below, our model and approach is identical to what we have described in our earlier publications. [12, 13, 15]

Since we are dealing with multiple polymer chains, we consider both interchain and intrachain single particle contributions. For the intrachain terms, we use the hopping terms and site energies derived for isolated polymer chains of a given species,  $t_{i,||}$ , where our notation denotes the parallel hopping term for the  $i$ th chain ( $i = 1, 2$ ). For PPV and similar conjugated polymer species, these are approximately 0.5eV for both valence and conduction  $\pi$  bands.

We include two intramolecular optical phonon branches which correspond roughly to the high-frequency C=C bond stretching modes within a given repeat unit and a second low-frequency mode, which in the case of PPV are taken to represent the phenylene torsional modes. The electron-phonon couplings are assumed to be transferable between the various chemical species. Since the modes are assumed to be intramolecular, we do not include interchain couplings in the phonon Hessian matrix.

Upon transforming  $H$  into the diabatic representation by diagonalizing the electronic terms at  $q_{i\mu} = 0$ , we obtain a series of vertical excited states  $|a_o\rangle$  with energies,  $\varepsilon_a^\circ$  and normal modes,  $Q_\xi$  with frequencies,  $\omega_\xi$ . (We will assume that the sum over  $\xi$  spans all phonon branches).

$$H = \sum_a \varepsilon_a^\circ |a_o\rangle \langle a_o| + \sum_{ab\xi} g_{ab\xi}^\circ q_\xi (|a_o\rangle \langle b_o| + |b_o\rangle \langle a_o|)$$

$$+ \frac{1}{2} \sum_{\xi} (\omega_{\xi}^2 Q_{\xi}^2 + P_{\xi}^2). \quad (2)$$

The adiabatic or relaxed states can be determined then by iteratively minimizing  $\varepsilon_a(Q_{\xi}) = \langle a|H|a \rangle$  according to the self-consistent equations

$$\frac{d\varepsilon_a(Q_{\xi})}{dQ_{\xi}} = g_{aa\xi} + \omega_{\xi}^2 Q_{\xi} = 0. \quad (3)$$

Thus, each diabatic potential surface for the nuclear lattice motion is given by

$$\varepsilon_a(Q_{\xi}) = \varepsilon_a + \frac{1}{2} \sum_{\xi} \omega_{\xi}^2 (Q_{\xi} - Q_{\xi}^{(a)})^2. \quad (4)$$

While our model accounts for the distortions in the lattice due to electron/phonon coupling, we do not account for any adiabatic change in the phonon force constants within the excited states.

While following along a relaxation pathway, crossing between diabatic states can occur. In order to insure maximum correlation between the relaxed state,  $\psi_b(Q_{\xi})$  and its parent vertical state  $\psi_{ao}(0)$ , we compute the inner product,  $S_{ab} = \langle \psi_{ao}(0) | \psi_b(Q_{\xi}) \rangle$  and select the state with the greatest overlap with the parent diabatic state. This allows us to follow a given state and correlate the adiabatic states with the parent vertical states. Figures 9 and 11 are examples of this. The dashed lines connect the parent vertical state with the final relaxed adiabatic state. We will comment upon these figures later in this paper.

Since we are dealing with inter-chain couplings we make the following set of assumptions. First, the single-particle coupling between chains is expected to be small compared to the intramolecular coupling. For this, we assume that the perpendicular hopping integral  $t_{\perp} = 0.01eV$ . This is consistent with LDF calculations performed by Vogl and Campbell and with the  $t_{\perp} \approx 0.15f_1$  estimate used in an earlier study of interchain excitons by Yu *et al.*[16, 17] Furthermore, we assume that the  $J(r)$ ,  $K(r)$ , and  $D(r)$  two-particle interactions depend only upon the linear distance between two sites, as in the intrachain case. Since these are expected to be weak given that the interchain separation,  $d$ , is taken to be some what greater than the inter-monomer separation. The third approximation that we make takes into account the difference in size of the repeat units of the polymer chains. As indicated in Fig. 1, the monomeric unit in BBL is roughly two times the size as a PPV monomeric unit. Thus, for the PPV:BBL junction we adopt the modified ladder scheme show in Fig. 2.

Finally, the most important assumption that we make is that the site energies for the electrons and holes for the various chemical species can be determined by comparing the relative HOMO and LUMO energies to PPV. These are listed in Table I. For example, the HOMO energy for PPV (as determined by its ionization potential) is -5.1eV. For BBL, this energy is -5.9 eV. Thus, we assume

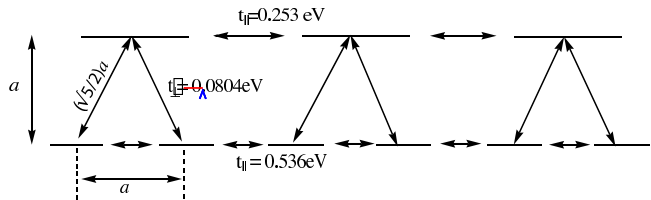


FIG. 2: Modified ladder coupling scheme for BBL:PPV inter-chain interactions. The parallel and perpendicular hopping integrals ( $t_{\parallel}$  and  $t_{\perp}$ ) for the two chains and the separation distances (in units of lattice spacing  $a$ ) are indicated on this figure. For the polymers under consideration, the top chain represents the BBL, chain while the sites correspond to the PPV chain.

that the  $\bar{f}_o$  for a hole on a BBL chain is 0.8 eV lower than  $\bar{f}_o$  for PPV at -3.55eV. Likewise for the conduction band. The LUMO energy of PPV is -2.7eV and that of BBL is -4.0eV. Thus, we shift the band center of the BBL chain 1.3eV lower than then PPV conduction band center to 1.45eV. For the F8BT, TFB, and PFB chains, we adopt a similar scheme as discussed below. The site energies and transfer integrals used throughout are indicated in Table I. We believe our model produces a reasonable estimate of the band off-sets in the PN-junctions formed at the interface between these semiconducting polymers.

### III. EXCITONIC VS. CHARGE SEPARATED STATES IN DONOR/ACCEPTOR POLYMER JUNCTIONS

#### A. Electronic States of Isolated Chains

Before moving on to consider the electronic states of the heterojunction systems, we make a brief examination of the CI states of the isolated chains. The relevant data for the vertical and adiabatic excitonic and charge-separated states are given in Table II. Since we have assumed a symmetric band structure,  $f_1 = -\bar{f}_1$ , the electron/hole wavefunctions will have even or odd symmetry under spatial inversion. Hence the total hamiltonian can be block diagonalized into even and odd parity blocks. The even parity states we term XT states since these are optically coupled to the ground state and are dominated by geminate electron/hole configurations. On the other hand, the odd-parity states are purely charge-separated states (CT) which possess no geminate electron/hole configurations, are optically coupled weakly at best to the ground state. We define the exciton binding energy to be the energy difference between the lowest energy XT and CT states. In each of the model systems considered, we obtain an exciton binding energy between 0.5 and 0.65V.

A uniform site model for F8BT, TFB, and PFB, may be a gross simplification of the physical systems. For

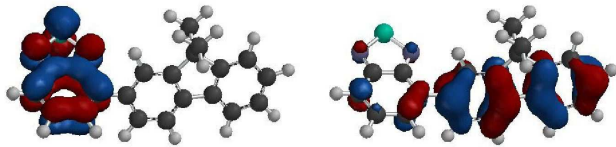


FIG. 3: Semiempirical (PM3) LUMO (left) and HOMO (right) orbitals for FBT monomer.

example, recent semi-empirical CI calculations by Jespersen, *et al.*[18] indicate that the lowest energy singlet excited state of F8BT consists of alternating positive and negative regions corresponding to the electron localized on the benzothiadiazole units and the hole localized on the fluorene units. These are consistent with a previous study by Cornil *et al.*[19] which places the LUMO on the benzothiadiazole units. Cornil *et al.*[19] also report the HOMO and LUMO levels of the isolated fluorene and benzothiadiazole Ref. [19] indicating a  $\Delta = 1.56$  eV off-set between the fluorene and benzothiadiazole LUMO levels and a 0.66 eV off-set between the fluorene and benzothiadiazole HOMO energy levels. Similarly, PM3 level calculations at the optimized geometry indicate a LUMO offset of 1.48eV and a HOMO offset of 0.8eV. The HOMO and LUMO orbitals for FBT (where we replaced the octyl side chains in F8BT with methyl groups) are shown in Fig. 3. This clearly indicates the localization of the HOMO and LUMO wave functions on the co-polymer units.

We can include this alternation into our model by modulating the site energies of the F8BT chain[13]. Thus, in F8BT we include a 0.5 eV modulation of both the valence and conduction band site energies relative to the band center. Table I. Hence, the fluorene site energies are at 2.42eV and -3.04eV for the conduction and valence band while the benzothiadiazole site energies are 1.42eV and -4.04eV. This results in a shift in the excitation energy to 0.28 eV relative to the unmodulated polymer and a 0.09 eV increase in the exciton binding energy. Furthermore, the absorption spectrum consists of two distinct peaks at

TABLE II: Vertical and Adiabatic singlet exciton energies for isolated polymer chains.

Molecule	length	$\epsilon_{EX}^{\circ}$	$\epsilon_{EX}$	$\epsilon_{CT}^{\circ}$	$\epsilon_{CT}$	$\epsilon_B$
PPV	10	2.56 eV	2.37 eV	3.01 eV	2.877 eV	0.51 eV
BBL	5	3.34	3.07	3.80	3.64	0.58
F8BT	10	2.28	2.12	2.79	2.71	0.59
PFB	10	2.94	2.744	3.37	3.23	0.49
TFB	10	3.15	2.96	3.59	3.45	0.49

$\epsilon_{XT}^{\circ}$ : vertical symmetric exciton energy,  
 $\epsilon_{XT}$ : adiabatic symmetric exciton energy,  
 $\epsilon_{CT}^{\circ}$ : vertical asymmetric exciton energy,  
 $\epsilon_{CT}$ : adiabatic asymmetric exciton energy,  
 $\epsilon_B$ : adiabatic exciton binding energy.

2.14eV (563nm) and 4.4eV (281nm) which are more or less on par with the 2.77eV (448nm)  $S_0 \rightarrow S_1$  and the 4.16eV (298 nm)  $S_0 \rightarrow S_9$  transitions computed by Jespersen *et al.* [18] and observed at 2.66eV and 3.63eV by Stevens, *et al.* [20].

The charge-separated character of the lowest singlet excited state of the F8BT-mod chain is readily apparent in Fig. 5 A and B. This is the state which give rise to the absorption maxima at 2.14 eV and is the only state present in the emission spectra. The odd-numbered sites are fluorene-sites and the even-numbered sites are benzothiadiazole sites. The alternating maxima in Fig. 5 A and B show that the hole is largely localized on the odd-sites and the electron is localized on the even-sites. The relaxed state is a self-trapped state with the electron largely localized on site 6 and the hole distributed on either side on sites 5 and 7. States C and D are the vertical and relaxed odd-parity state corresponding to a dissociated charge-transfer state. Finally, E and F in this figure correspond to the state responsible for the absorption peak at 4.4eV. In this state, the electron and hole are more or less uniformly delocalized over the entire polymer segment and carries an oscillator strength comparable to the 2.14eV state, again consistent with the semiempirical data. [18]

For PFB and TFB monomers, semiempirical (PM3) calculations at the ground state equilibrium configuration give HOMO energies of -8.00748eV and -7.95994 eV and LUMO energies of -0.01862 eV and 0.05201 eV

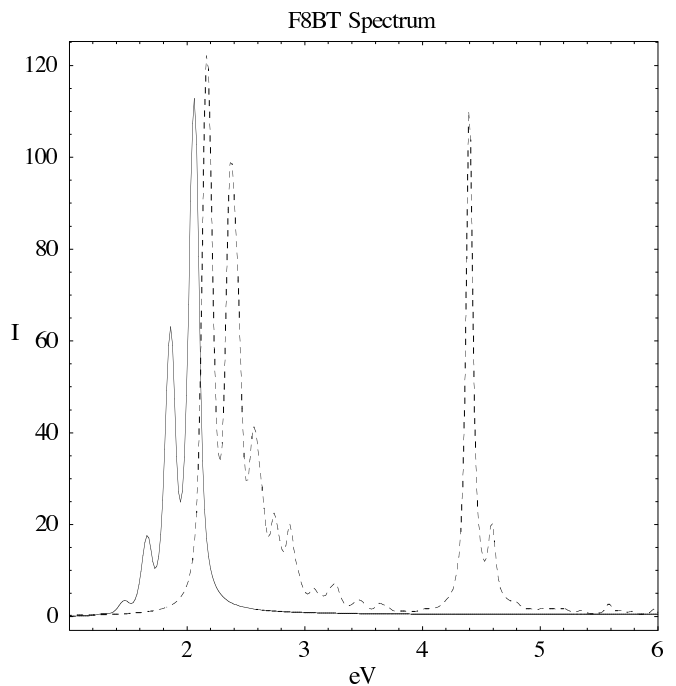


FIG. 4: Absorption (dashed) and vibronic emission (solid) spectra for the modulated F8BT chain. The vibronic fine-structure in each peak is due to the C=C bond-stretching phonon branch.

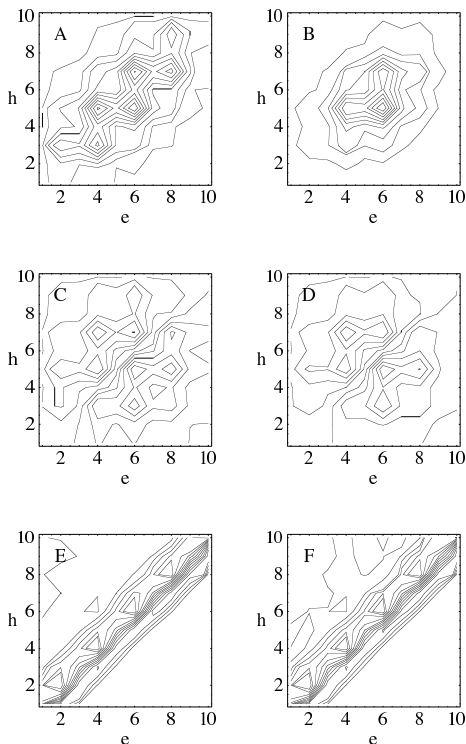


FIG. 5: Vertical (A,C,D) and relaxed (B,D,F) electron/hole densities for modulated F8BT chain (F8BT-mod). A,B) Exciton, C,D.) Asymmetric Charge-transfer state, E,F)  $\pi^*$  Exciton. States A,B and E, F correspond to the  $S_1$  CT and  $S_0$   $\pi \rightarrow \pi^*$  states reported in Ref. [18].

respectively for isolated phenylenediamine and diphenylamine units. In comparison, the semiempirical HOMO and LUMO levels for the fluorene segment are  $-8.83304\text{eV}$  and  $-0.32915\text{eV}$ , respectively. In the combined copolymers, the LUMO is more or less localized on the fluorene as in the F8BT case as shown in Fig. 6. To account for this modulation within our model, we include an  $0.2\text{eV}$  modulation about the band centers listed in Table I in the conduction and valence site energies for the PFB and TFB chains. Since the net modulation is on the order of the exciton binding energy, the the electron and hole will be localized on alternate repeat units in the lowest excited state as indicated in Fig. 7-A for the vertical exciton and Fig. 7-B for the adiabatic or self-trapped exciton. Even though the electron and hole are on different lattice sites, they remain a bound pair. Fig. 7-C and -D show the dissociated electron/hole pair as evidenced by the nodal line along the  $e = h$  diagonal.

Table II summarizes the relevant states for the isolated chains discussed in this paper. It is interesting to note that for the unmodulated chains (PPV and BBL) the adiabatic exciton binding energy is  $0.1\text{eV}$  higher than in the modulated co-polymer chains (F8BT, TFB, and PFB). Having established models for the electronic states of the isolated chains, we turn our attention towards modeling the electronic states of the polymer heterojunctions.

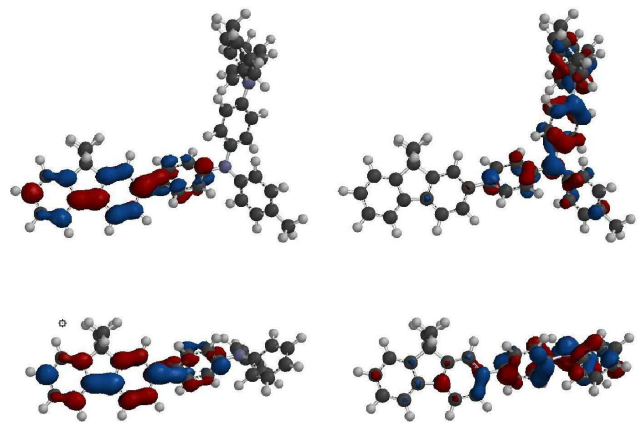


FIG. 6: (color online) Semiempirical (PM3) LUMO (left) and HOMO (right) wave functions for PFB (top) and TFB (bottom) monomer

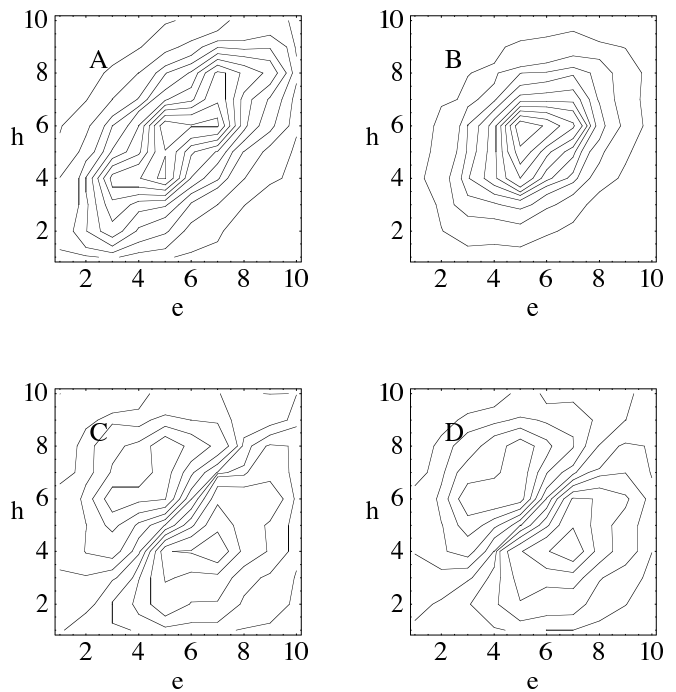


FIG. 7: Vertical and adiabatic exciton (A,B) and charge-separated states (C,D) for the 10 site TFB chain. See text for details.

## B. Electronic states of heterojunctions

We consider three model heterojunction systems: PPV:BBL, TFB:F8BT, and PFB:F8BT. As discussed in the introduction, devices fabricated using these polymers are either layered nanostructures or phase-separated polymer blends. The crucial energetic consideration is the exciton destabilization threshold. In an ideal non-interaction electron model, a type II heterojunction will destabilize an exciton present at the interface if the exciton binding energy is less than the band-off set. In

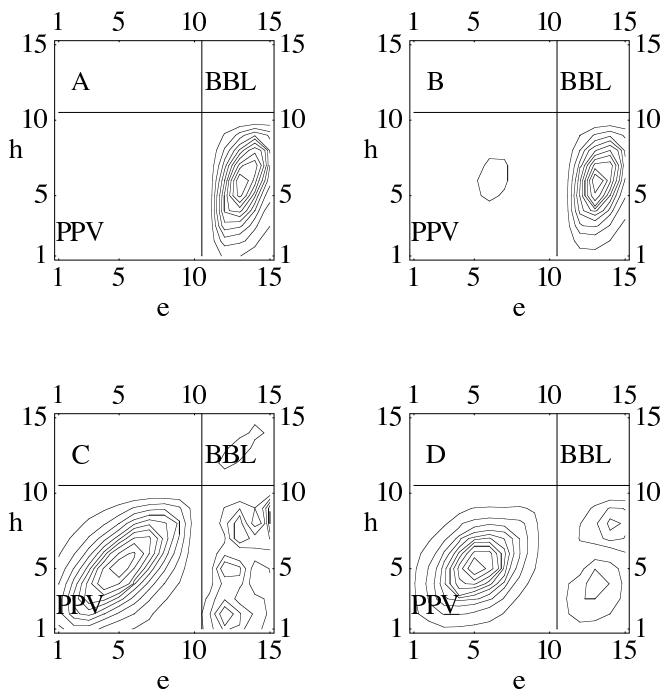


FIG. 8: Excited state electron/hole densities for PPV:BBL heterojunction. The axes "e" and "h" refer to the electron and hole "coordinates" on the lattice. Sites 1-10 are the PPV sites and sites 11-15 are the BBL sites. Plots A and B show the density for the lowest energy vertical and adiabatically relaxed charge-transfer state while C and D correspond to the vertical and relaxed density for the excitonic state indicated in the correlation diagram. In C and D one can clearly see the mixing between the intrachain exciton on PPV and interchain charge-separated configuration with the hole residing on PPV and the electron being transferred to the BBL.

organic semiconductors, the Coulombic interaction between the electron and the hole is quite significant with exciton binding energies in excess of 0.5 eV in most materials. When this is on the order of the band off-set, excitons can be stable at the interface giving LED behavior. By selecting materials with different HOMO and LUMO energies, one can effectively tune LED or photovoltaic performance of a heterojunction material.

### 1. PPV:BBL

The first of these semiconductor heterojunction materials we consider here, PPV:BBL, has been used in the fabrication of solar-cells and photovoltaic devices and a recent review by Alam and Jenehke provide a succinct overview of recent progress towards the fabrication of efficient solar-cell devices using layers of organic polymer donor/acceptor heterojunction materials.[2, 3, 5, 6, 21, 22, 23, 24, 24, 25, 26, 27, 28, 29, 30, 31, 32, 33, 34, 35, 36] By alternating nanoscale bilayers of high electron affinity (EA) acceptor polymers such as BBL with an EA = 4.0eV with a donor such as PPV or its soluble derivative MEH-

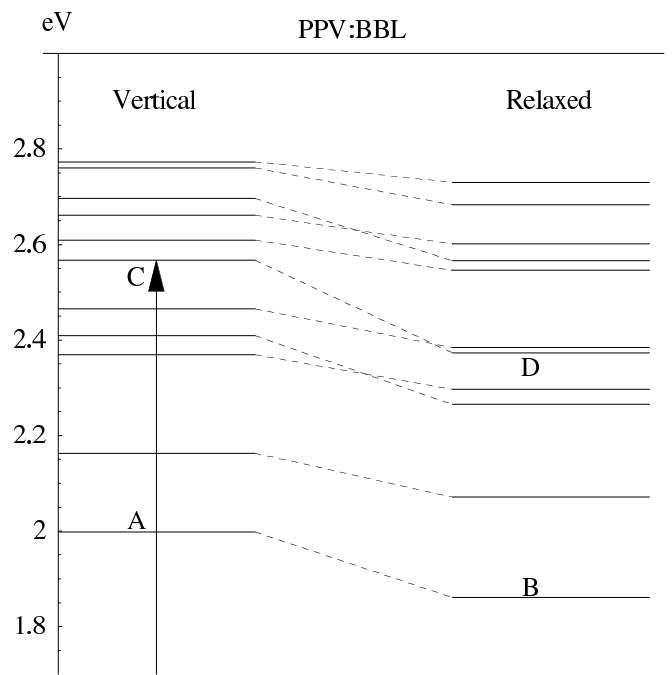


FIG. 9: Correlation between vertical and adiabatic energy levels for the PPV:BBL heterojunction. The vertical scale is the excitation energy. Labeled states correspond to densities plotted in Fig. 8.

PPV exhibit rapid and efficient photoinduced charge transfer and large photovoltaic power conversions under white light illumination at 80-100 m/cm<sup>2</sup> (AM1.5).[5] Since the band off-set at the heterojunction of the materials is larger than the exciton binding energy in PPV:BBL, photoexcitation of either BBL or PPV will result in the production of a charge-separated interchain species.

The relevant states for the PPV:BBL heterojunction are shown in Fig. 8. The top two figures are electron/hole densities for inter-chain charge-separated state while the bottom two are the vertical and adiabatic densities for the exciton. Fig. 9 indicates the correlation between the vertical and relaxed energy levels. The vertical exciton (Fig. 8-C) corresponds to the state with the largest transition dipole to the  $S_0$  ground state.

First, we note that the lowest energy excited state in this system is the charge-transfer state in which the hole resides on the PPV chain (sites 1-10 in Fig. 8) and the electron resides on the BBL chain (sites 11-15). There is some mixing between the interchain charge-transfer state and geminate electron/hole configurations on either chain as evidenced by the smallest contour rings in Fig. 8 A and B. Clearly, >99.9% of the population is in interchain charge-transfer configurations. The vertical excitonic state, Fig. 8 C, is largely localized on the PPV chain with some mixing between the chains. We find that the extent of the interchain mixing is determined largely by the interchain hopping integral, which we set at  $t_{\perp} = 0.15t_{\parallel} = 0.0804eV$ . In the self-trapped exciton (Fig. 8 D), the interchain mixing is weaker.

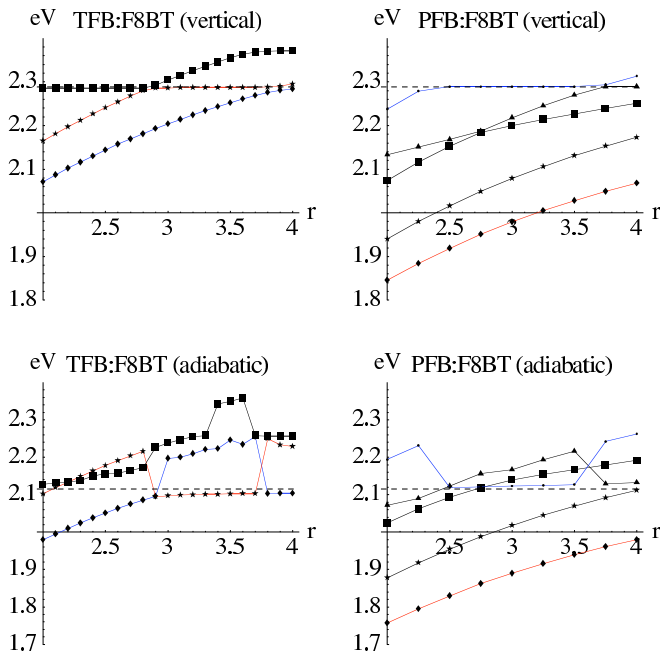


FIG. 10: Variation of vertical CI energy levels for cofacial PFB:F8BT and TFB:F8BT chains with chain separation,  $r$ , taken units of the lattice constant,  $a$ . The horizontal dashed line corresponds to the exciton energy level for the isolated F8BT chain.

The energy level diagram shown in Fig.9 shows the correlation between the vertical excited states (at the ground state equilibrium geometry ( $Q_\mu = 0$ ) with the adiabatically relaxed excited states, each of which has a unique excited state equilibrium geometry. This correlation diagram indicates a number of intersystem crossings can occur as the system relaxes from the vertical to adiabatic geometries. In particular, notice that the excitonic state (C) intersects another state as it relaxes to D. This state is nearly degenerate with the adiabatic exciton (D) and is predominantly an interchain charge-transfer state. It is interesting to speculate the role that such intersections and close degeneracies will play in the photophysics of this system.

## 2. PFB:F8BT vs. TFB:F8BT

As discussed earlier, TFB:F8BT and PFB:F8BT sit on either side of the exciton destabilization threshold. In TFB:F8BT, the band off-set is less than the exciton binding energy and these materials exhibit excellent LED performance. On the other hand, devices fabricated from PFB:F8BT where the exciton binding energy is less than the off-set, are very poor LEDs but hold considerable promise for photovoltaic devices. In both of these systems, the lowest energy state is assumed to be an interchain exciplex as evidenced by a red-shifted emission about 50-80ns after the initial photoexcitation. [9] In the case of TFB:F8BT, the shift is reported to be  $140 \pm 20$

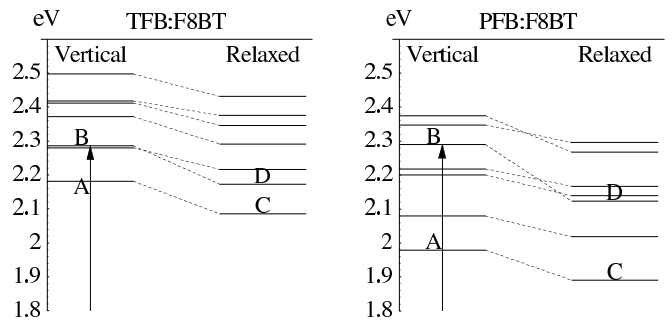


FIG. 11: Correlation between vertical and adiabatic energy levels for TFB:F8BT and PFB:F8BT heterojunctions. The vertical scale is the excitation energy in eV. Up and down arrows correspond to states present in absorption or emission spectra of each heterojunction. In PFB:F8BT, the lowest energy state is dark. The levels labeled A-D correspond to the states plotted in Fig. 12 and Fig. 13.

meV and in PFB:F8BT the shift is  $360 \pm 30$  meV relative to the exciton emission, which originates from the F8BT phase. Bearing this in mind, we systematically varied the separation distance between the cofacial chains from  $r = 2a - 5a$  (where  $a =$  unit lattice constant) and set  $t_\perp = 0.01$  in order to tune the Coulomb and exchange coupling between the chains and calibrate our parameterization. Fig. 10 shows the variation of the lowest few diabatic states with  $r$  for both heterojunctions. The dashed line in each corresponds to the exciton energy for an isolated F8BT chain. For large interchain separations, the exciton remains localized on the F8BT chain in both cases. As the chains come into contact, dipole-dipole and direct Coulomb couplings become significant and we begin to see the effect of exciton destabilization. For TFB:F8BT, we select and interchain separation of  $r = 2.8a$  giving a 104meV splitting between the vertical exciton and the vertical exciplex and 87.4 meV for the adiabatic states. For PFB:F8BT, we chose  $r = 3a$  giving a vertical exciton-exciplex gap of 310 meV and an adiabatic gap of 233 meV. In both TFB:F8BT and PFB:F8BT, the separation produce interchain exciplex states as the lowest excitations. with energies reasonably close to the experimental shifts.

Fig. 11 compares the vertical and adiabatic energy levels in the TFB:F8BT and PFB:F8BT chains and Figs. 12 and 13 show the vertical and relaxed exciton and charge-separated states for the two systems. Here, sites 1-10 correspond to the TFB or PFB chains and 11-20 correspond to the F8BT chain. The energy levels labeled in Fig. 11 correspond to the states plotted in Figs. 12 and 13. We shall refer to states A and B as the vertical exciplex and vertical exciton and to states C and D as the adiabatic exciplex and adiabatic exciton respectively. Roughly, speaking a pure exciplex state will have the charges completely separated between the chains and will contain no geminate electron/hole configurations. Likewise, strictly speaking, a pure excitonic state will be localized to a single chain and have only geminate elec-

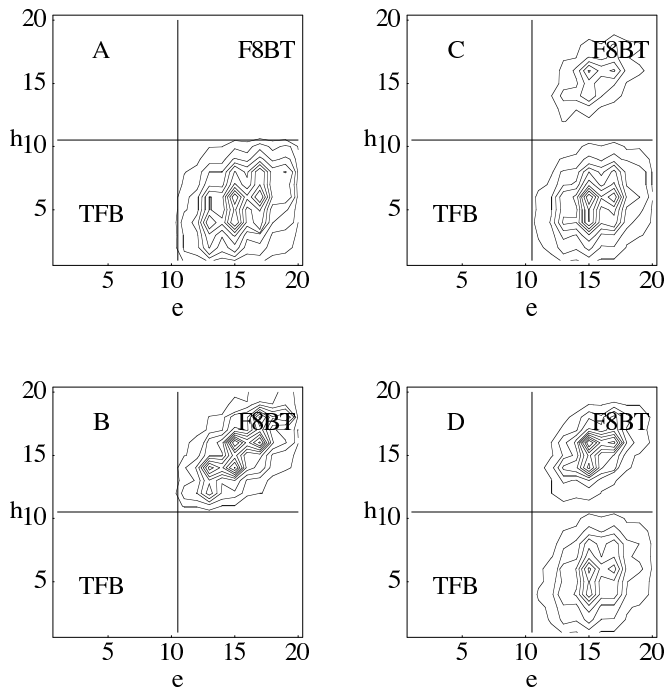


FIG. 12: Excited state electron/hole densities for TFB:F8BT heterojunction. The electron/hole coordinate axes are the same as in Fig. 8 except that sites 1-10 correspond to TFB sites and 11-20 correspond to F8BT sites. Note the weak mixing between the interchain charge-separated states and the F8BT exciton in each of these plots.

tron/hole configurations. Since site energies for the the F8BT chain are modulated to reflect to internal charge-separation in the F8BT co-polymer as discussed above, we take our “exciton” to be the lowest energy state that is localized predominantly along the diagonal in the F8BT “quadrant”.

In the TFB:F8BT junction, the lowest excited state is the exciplex for both the vertical and adiabatic lattice configurations with the hole on the TFB and the electron on the F8BT. (Fig.12A,C) In the vertical case, there appears to be very little coupling between intrachain and interchain configurations. However, in the adiabatic cases there is considerable mixing between intra- and inter-chain configurations. First, this gives the adiabatic exciplex an increased transition dipole moment to the ground state. Secondly, the fact that the adiabatic exciton and exciplex states are only 87 meV apart means that at 300K, about 4% of the total excited state population will be in the adiabatic exciton.

For the PFB:F8BT heterojunction, the band off-set is greater than the exciton binding energy and sits squarely on the other side of the stabilization threshold. Here the lowest energy excited state (Figs. 13A and B) is the interchain charge-separated state with the electron residing on the F8BT (sites 11-20 in the density plots in Fig 13) and the hole on the PFB (sites 1-10). The lowest energy exciton is almost identical to the exciton in the TFB:F8BT

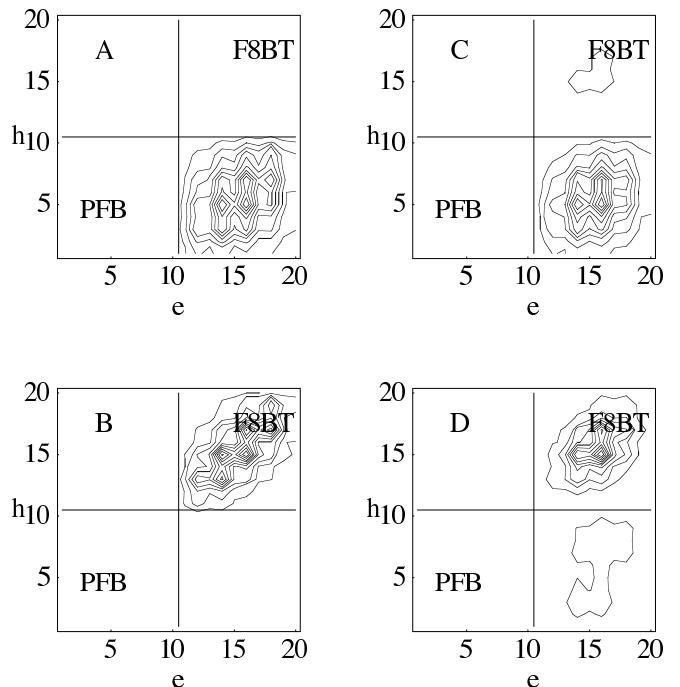


FIG. 13: Excited state electron/hole densities for PFB:F8BT heterojunction. The axes are as in previous figures except that sites 1-10 correspond to PFB sites and sites 11-20 to F8BT sites.

case. Remarkably, the relaxed exciton (Fig. 13D) shows slightly more interchain charge-transfer character than the vertical exciton (Fig. 13C). While the system readily absorbs at 2.3eV creating a localized exciton on the F8BT, luminescence is entirely quenched since all population within the excited states is readily transfer to the lower-lying interchain charge-separated states with vanishing transition moments to the ground state.

The mixing between the exciplex and exciton in TFB:F8BT can be seen in the predicted emission spectra for the system. Fig. 14 shows the absorption and emission spectra for the TFB:F8BT and PFB:F8BT computed by taking the transition dipole moment between the vertical and relaxed excited states to the ground state. While the fluorescent emission from TFB:F8BT is weaker than the corresponding absorption, it is not entirely quenched as in the PFB:F8BT case.

#### IV. DISCUSSION

In this paper, we developed a model for donor-acceptor semiconducting polymer heterojunctions. For the PPV:BBL heterojunction, the band off-sets at the polymer interface is sufficient to dissociate an electron/hole pair created by photoexcitation. Because of this natural internal driving force to create charge-separated states, PPV:BBL blends are of considerable interest to materials chemists and device engineers de-



veloping efficient photovoltaic cells for solar energy conversion [5]. TFB:F8BT and PFB:F8BT are very similar heterojunctions. Within our model, the single parametric difference between TFB and PFB is the location of the band-center for the valence band. In TFB:F8BT, the off-set between the valence bands is  $(-2.98\text{eV} + 3.54\text{eV})$   $0.56\text{eV}$  which is right at the exciton binding energy. Hence, we see considerable mixing between the intrachain exciton localized on the F8BT and a charge-separated state. In the PFB-F8BT case, the valence band off-set is  $0.79\text{ eV}$ , clearly greater than the exciton binding energy. Hence, the lowest energy excited states are predominantly interchain charge-separated states.

In a forthcoming paper, [11], we continue along the lines set forth in this paper by computing the state-to-state relaxation dynamics following both photoexcitation and electron/hole injection. We will compare results obtained within a vertical approximation (whereby transitions occur via phonon creation/annihilation, but the lattice is frozen in the ground-state equilibrium geometry) to those obtained within an adiabatic Marcus-Jortner-Hush approximation where the transitions occur between the equilibrium geometry of each excited state. We will also discuss the role that the avoided crossings and conical intersections of the Born-Oppenheimer potential energy surfaces of the excited states play in the

electron/hole capture process, exciplex formation, and in the thermal regeneration of intramolecular excitons in TFB:F8BT.

### Acknowledgments

This work was supported in part by the National Science Foundation and the Robert A. Welch Foundation.

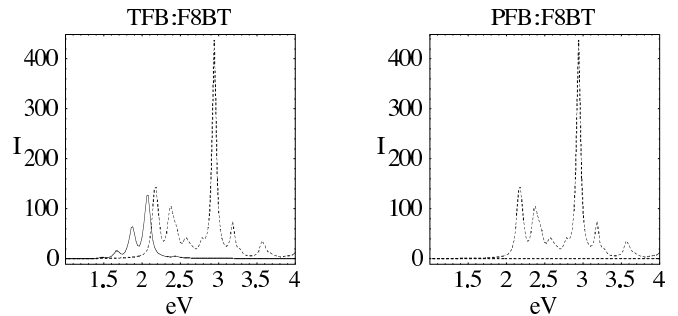


FIG. 14: Vibronic absorption (dashed) and emission (solid) spectra of TFB:F8BT and PFB:F8BT heterojunctions. Note that in the TFB:F8BT the fluorescence spectrum is scaled by a factor of 100.

- 
- [1] C. W. Tang, Applied Physics Letters **48**, 183 (1986), URL <http://link.aip.org/link/?APL/48/183/1>.
- [2] M. Granström, K. Petritsch, A. Arais, A. Lux, M. Andersson, and R. H. Friend, Nature **395**, 257 (1998).
- [3] U. Bach, D. Lupo, P. Comte, J. E. Moser, F. Weissörtel, H. S. J. Salbeck, and M. Grätzel, Nature **395**, 583 (1998).
- [4] W. Shockley, *Electrons and Holes in Semiconductors* (van Norstrand, 1950).
- [5] M. M. Alam and S. A. Jenekhe, Chem. Matter. **16**, 4647 (2004).
- [6] G. Yu, J. Gao, J. C. Hummelen, F. Wudl, and A. J. Heeger, Science **270**, 1789 (1995), URL <http://www.sciencemag.org/cgi/content/abstract/270/5243/1789>.
- [7] J. J. M. Halls, C. A. Walsh, N. C. Greenham, E. A. Marseglia, R. H. Friend, S. C. Moratti, and A. B. Holmes, Nature **376**, 498 (1995).
- [8] J. J. M. Halls, J. Cornil, D. A. dos Santos, R. Silbey, D.-H. Hwang, A. B. Holmes, J. L. Bredas, and R. H. Friend, Physical Review B (Condensed Matter and Materials Physics) **60**, 5721 (1999), URL <http://link.aps.org/abstract/PRB/v60/p5721>.
- [9] A. C. Morteani, A. S. Dhoot, J.-S. Kim, C. Silva, N. C. Greenham, C. Murphy, E. Moons, S. Cina, J. H. Burroughes, and R. H. Friend, Adv. Mater. **15**, 1708 (2003).
- [10] A. C. Morteani, P. Sreearunothai, L. M. Herz, R. H. Friend, and C. Silva, Physical Review Letters **92**, 247402 (pages 4) (2004), URL <http://link.aps.org/abstract/PRL/v92/e247402>.
- [11] E. R. Bittner, J. G. S. Ramon, and S. Karabunarliev, J. Chem. Phys. in preparation (2005).
- [12] S. Karabunarliev and E. R. Bittner, The Journal of Chemical Physics **118**, 4291 (2003), URL <http://link.aip.org/link/?JCP/118/4291/1>.
- [13] S. Karabunarliev and E. R. Bittner, J. Phys. Chem. B **108**, 10219 (2004), URL <http://pubs.acs.org/cgi-bin/abstract.cgi/jpcbfk/2004/108/12>.
- [14] S. Karabunarliev and E. R. Bittner, Physical Review Letters **90**, 057402 (pages 4) (2003), URL <http://link.aps.org/abstract/PRL/v90/e057402>.
- [15] S. Karabunarliev and E. R. Bittner, The Journal of Chemical Physics **119**, 3988 (2003), URL <http://link.aip.org/link/?JCP/119/3988/1>.
- [16] P. Vogl and D. K. Campbell, Phys. Rev. B **41**, 12797 (1990).
- [17] Z. G. Yu, M. W. Wu, X. S. Rao, X. Sun, and A. R. Bishop, J. Phys.: Condens. Matter **8**, 8847 (1996).
- [18] K. G. Jespersen, W. J. D. Beenken, Y. Zaushitsyn, A. Yartsev, M. Andersson, T. Pullerits, and V. Sundstrom, The Journal of Chemical Physics **121**, 12613 (2004), URL <http://link.aip.org/link/?JCP/121/12613/1>.
- [19] J. Cornil, I. Gueli, A. Dkhissi, J. C. Sanchez-Garcia, E. Hennebicq, J. P. Calbert, V. Lemaure, D. Beljonne, and J. L. Bredas, The Journal of Chemical Physics **118**, 6615 (2003), URL <http://link.aip.org/link/?JCP/118/6615/1>.
- [20] M. A. Stevens, C. Silva, D. M. Russell, and R. H. Friend, Physical Review B (Condensed Matter and Materials Physics) **63**, 165213 (pages 18) (2001), URL <http://link.aps.org/abstract/PRB/v63/e165213>.
- [21] S. A. J. and John A. Osaheni, Science **265**, 765 (1994).

- [22] I. Kamohara, M. Townsend, and B. Cottle, *Journal of Applied Physics* **97**, 014501 (pages 9) (2005), URL <http://link.aip.org/link/?JAP/97/014501/1>.
- [23] D. M. Russell, A. C. Arias, R. H. Friend, C. Silva, C. Ego, A. C. Grimsdale, and K. Mullen, *Applied Physics Letters* **80**, 2204 (2002), URL <http://link.aip.org/link/?APL/80/2204/1>.
- [24] S. A. Jenekhe and S. Yi, *Applied Physics Letters* **77**, 2635 (2000), URL <http://link.aip.org/link/?APL/77/2635/1>.
- [25] X. L. Chen and S. A. Jenekhe, *Applied Physics Letters* **70**, 487 (1997), URL <http://link.aip.org/link/?APL/70/487/1>.
- [26] L.-B. Lin, S. A. Jenekhe, and P. M. Borsenberger, *Applied Physics Letters* **69**, 3495 (1996), URL <http://link.aip.org/link/?APL/69/3495/1>.
- [27] X. Weng, Y. Kostoulas, P. M. Fauchet, J. A. Osaheni, and S. A. Jenekhe, *Physical Review B (Condensed Matter)* **51**, 6838 (1995), URL <http://link.aps.org/abstract/PRB/v51/p6838>.
- [28] J. Xue, S. Uchida, B. P. Rand, and S. R. Forrest, *Applied Physics Letters* **84**, 3013 (2004), URL <http://link.aip.org/link/?APL/84/3013/1>.
- [29] J. A. Osaheni, S. A. Jenekhe, and J. Perlstein, *Applied Physics Letters* **64**, 3112 (1994), URL <http://link.aip.org/link/?APL/64/3112/1>.
- [30] J. Gao and J. Dane, *Applied Physics Letters* **84**, 2778 (2004), URL <http://link.aip.org/link/?APL/84/2778/1>.
- [31] B. A. Gregg, S. Ferrere, and F. Pichot, in *Interfacial processes in organic-based solar cells*, edited by Z. H. Kafafi and D. Fichou (SPIE, 2002), vol. 4465, pp. 31–42, URL <http://link.aip.org/link/?PSI/4465/31/1>.
- [32] K. Saito and M. Sugi, *Applied Physics Letters* **61**, 116 (1992), URL <http://link.aip.org/link/?APL/61/116/1>.
- [33] A. G. Manoj, A. A. Alagiriswamy, and K. S. Narayan, *Journal of Applied Physics* **94**, 4088 (2003), URL <http://link.aip.org/link/?JAP/94/4088/1>.
- [34] K. S. Narayan, B. E. Taylor-Hamilton, R. J. Spry, and J. B. Ferguson, *Journal of Applied Physics* **77**, 3938 (1995), URL <http://link.aip.org/link/?JAP/77/3938/1>.
- [35] J.-I. Nakamura, C. Yokoe, K. Murata, and K. Takahashi, *Journal of Applied Physics* **96**, 6878 (2004), URL <http://link.aip.org/link/?JAP/96/6878/1>.
- [36] P. Schilinsky, C. Waldauf, J. Hauch, and C. J. Brabec, *Journal of Applied Physics* **95**, 2816 (2004), URL <http://link.aip.org/link/?JAP/95/2816/1>.